Supplement: Non-conventional colloidal aggregation in bacterial baths

Daniel Grober,[1,2] Ivan Palaia[1], Mehmet Can Ucar[1], Edouard Hannezo[1], Anđela Šarić[1], Jérémie Palacci[1,2*]

[1]Department of Physics, University of California - San Diego

[2]Institute of Science and Technology - Austria

[*]To whom correspondence should be addressed; E-mail: jeremie.palacci@ist.ac.at

Supplementary materials

Description of Movies

Supplementary Text

Fig. S1 to S13

References (17, 18, 23, 25, 26, 35-42)

Movie S1 - S8

Description of Movies

Movie S1: (Experiment) Comparison of aggregation in thermal versus active baths. Sticky colloids aggregate in either a thermal (ρ_B=0) or active bath of swimming *E. Coli* ($\rho_B = 0.5\rho^*$) - all other parameters being equal (same concentration of colloids, strength of attraction by depletion, objective and speed of acquisition). The field of view in each video is 650 x 650 μm. The dynamics appear much faster in the active bath than the thermal bath, and the morphology of the aggregates differ. Real time of the movie is 4h.

Movie S2: (Experiment) Persistent clockwise rotation of aggregates in the active bath. An accelerated video of sticky colloids in the active bath of swimming *E. Coli* ($\rho_B = \rho^*$) , which highlights the persistent clockwise motion of the aggregates. Real time of the movie is 2h.

Movie S3: (Simulation) Conventional aggregation in a thermal bath. Simulated aggregation of colloids with no internal activity (the internal torque for each particle is set to $0\,k_{\mathrm{B}}T$ [see SI]). The playback speed increases twice during the movie, at times 10000 and 50000, in order to capture both the formation of small aggregates at short times and the formation of large structures and gelification, occurring on long time scales. The time of each frame is indicated in the top right corner. Packing fraction $\Phi = 0.16$.

Movie S4: (Simulation) Aggregation at low activity. The internal torque for each particle is set to $1\,k_{\mathrm{B}}T$, [see SI]. Rotation and partial folding of the aggregates arise, resulting in faster and morphologically different aggregation, compared to the thermal case. The system percolates and forms a space-spanning network at large times. The playback speed increases twice during the movie, at times 10000 and 50000, in order to capture both the formation of small aggregates at short times and the formation of large structures and gelification, occurring on long time

scales. The time of each frame is indicated in the top right corner. Packing fraction $\Phi = 0.16$.

Movie S5: (Simulation) Aggregation at high activity. The internal torque for each particle is set to $10\,k_{\mathrm{B}}T$, [see SI]. Rotation and folding of the aggregates arise, resulting in faster and morphologically different aggregation, compared to the thermal case. The system does not percolate and the gel phase is replaced by compact clusters. The playback speed increases twice during the movie, at times 10000 and 50000, in order to capture both the formation of small aggregates at short times and the dynamics on long time scales. The time of each frame is indicated in the top right corner. Packing fraction $\Phi = 0.16$.

Movie S6: (Simulation) Zoomed in view of aggregation and folding at high activity. A subsection of the simulation window, focusing on the non-conventional aggregation of particles; the rotation and folding leads to the formation of a compact cluster (the internal torque for each particle is set to $10\,k_{\mathrm{B}}T$, [see SI]). The playback speed is constant, and the time of each frame is indicated in the top right corner. Packing fraction $\Phi = 0.16$.

Movie S7 (Simulation) Mechanical test of a gel assembled in thermal conditions. The gel was previously assembled with the internal torque for each particle is set to $0\,k_{\mathrm{B}}T$, [see SI], and the internal torque remains at $0\,k_{\mathrm{B}}T$ during the stretching experiment. The strain increases with time, and the exact value is indicated in the top right. The gel exhibits an elastic response in the considered regime of strain [see Main Text].

Movie S8 (Simulation) Mechanical test of a gel assembled in active conditions. The gel was previously assembled in active conditions (the internal torque for each particle is set to $3\,k_{\mathrm{B}}T$ [see SI]), and the internal torque is set to $0\,k_{\mathrm{B}}T$ during the stretching experiment. The strain

increases with time, and the exact value is indicated in the top right. The non-conventional aggregation in active conditions results in a gel with different structure, as compared with the gel assembled in thermal conditions (Movie S7); this results in a different mechanical response. Notably, the gel starts tearing at strain 0.089.

Supplemental Text

E. Coli Growth and Characterization

Growth

E. Coli (strain MG1655) are grown overnight until saturation at 33C, shaken at 200 RPM, in Tryptone Broth containing 10g/L Tryptone, and 5g/L NaCl. The saturated culture is diluted 1:100 into fresh Tryptone Broth and grown at 33C until optical density = 0.5, corresponding to mid-exponential growth phase. 1mL of cells are centrifuged at 2200 rpm for 10 min until a pellet forms. The supernatant is removed and the cells are gently re-suspended in Motility Medium (MM), containing 10mM Potassium Phosphate buffer (pH 7) and 0.1mM EDTA (pH 8). This process is repeated twice more, to ensure the growth media is sufficiently diluted. In the final step, the cells are re-suspended in 10% of the volume of the supernatant, to create a highly concentrated sample of cells.

Cell Counting

Optical Density is used to quantify the concentration of cells in a sample. This measurement is made by shining light through a cuvette of known size containing a suspension of cells. The optical density is obtained from the ratio of the light intensity output and the light intensity input, and related to the density of cells in the suspension through the below equation:

$$OD = \log_{10}(\frac{I}{I_0}) = \epsilon * l * \rho$$

Where ρ is the density of cells in suspension, l is the path length of the light and ϵ a constant which must be calibrated experimentally using cell counting experiments. We conducted these experiments by diluting a sample of *E. Coli* at a known Optical Density one part per million into Phosphate Buffered Saline Solution (PBS); 100uL of the diluted sample is then spread on an LB agar plate and left overnight at 33C. The following morning, individual colonies, originating

from a single cell, are counted by eye. The results of these experiments are summarized in Fig. S1; based on the data, we measure $OD1 = 7 \times 10^8 cells/mL$.

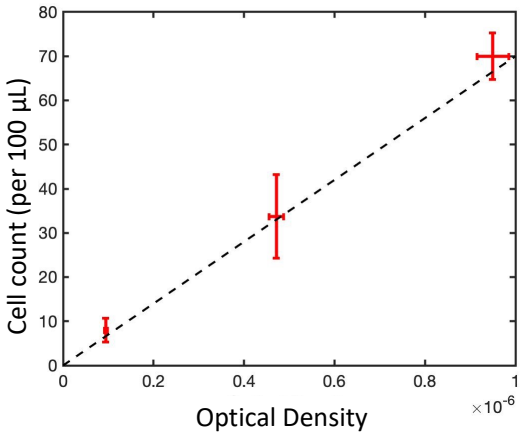

Figure S1 Results of the Cell Counting experiments, used to quantify the number of cells at a specific optical density. Data is binned, and the averages and standard deviations of those bins are displayed in red. The black line is an approximate fit to the data; we determine that $OD(1) = 7 \cdot 10^8 cells/mL$.

DDM

We use Dynamic Differential Microscopy (DDM) to characterize our active suspension of *E. Coli* [17, 18]. We capture 3000 frames at 20fps using a 10x Nikon objective (NA = 0.3) in the focal plane of the bottom of the glass capillary, using phase contrast microscopy. Videos are captured automatically at 3 different locations along the capillary, every 30 minutes, for 4 hours. The average velocity and fraction of *E. Coli* moving ballistically are reported in Fig. S2A and Fig. S2B, respectively.

To understand the effect of different environmental conditions on the motility of the *E. Coli*, we carry out three separate experiments. In each experiment, *E. Coli* cells are suspended in MM at a concentration of 6×10^8 cells/mL. 10mM NaCl and 0.1% F-108 and are added, in agreement with solution used for Colloidal Aggregation. We find that this solution is not sufficient to maintain motility over a period of 4 hours [Fig. S2A, red line]. Next, we add

1% w/v Glucose; *E. Coli* in these conditions maintain a constant speed of $16 \pm 1\mu m/s$ and constant fraction alive for at least 4 hours [Fig. S2A and Fig. S2B, green line]. Finally, we add both 1% w/v Glucose and 3.25g/L PEO, identical to the conditions in the colloidal aggregation experiment; we observe an increase in the average *E. Coli* swim speed to $23 \pm 2\mu m/s$, while the speed and fraction alive remain relatively constant over the four hours [Fig. S2A and Fig. S2B, blue line]. An increase in speed is consistent with previous literature regarding the effect of polymers on *E. Coli* motility [37].

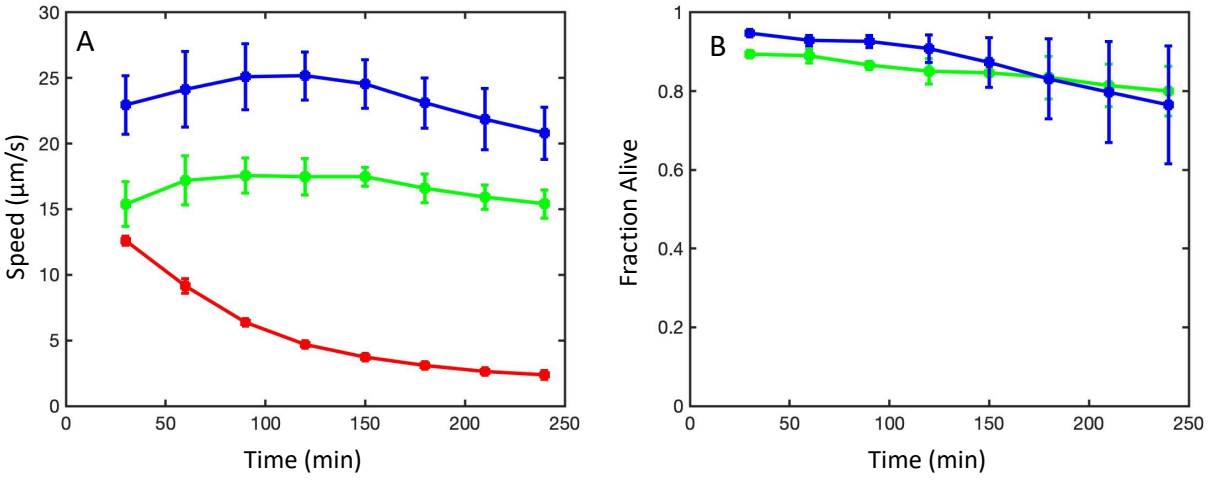

Figure S2 (A) *E. Coli* swim speed as a function of time, analyzed using the DDM technique. *E. Coli* motility is analyzed in three environmental conditions: Motility Medium (Red), Motility Medium and 1% w/v Glucose (Green), or Motility Medium, 1% w/v Glucose, and 3.25g/L PEO (Blue). (B) Fraction of *E. Coli* alive as a function of time, analyzed using the DDM technique. The *E. Coli* are suspended in Motility Medium and 1% w/v Glucose (Green), or Motility Medium, 1% w/v Glucose, and 3.25g/L PEO (Blue).

Colloidal Aggregation Experiments

Colloidal Aggregation Solution

Colloids (diameter 2.2 μm TPM Spheres) are diluted into solution containing Motility Medium (MM), 3.25g/L PEO, 10mM NaCl, 0.1% F108, and 1% Glucose. *E. Coli* cells are added from the high concentration sample of cells suspended in MM, described previously. To vary the strength of the active bath, we repeat the experiment with different bacteria concentrations. Bacteria concentrations are reported in fractions of the maximum concentration: $\rho^* = 6 \times 10^8 cells/mL$. The solution is confined in a 3mm x 0.3mm x 50mm rectangular glass capillary, utilizing capillarity, placed on a glass slide and sealed with a wax pen.

Short time dynamics: experiment set up

For experiments measuring the diffusion of colloidal aggregates, the concentration of colloids is chosen such that the surface area fraction is $10\% \pm 2\%$, once the colloids have sedimented onto the bottom surface of the glass capillary. We repeat the experiments at four *E. Coli* concentrations: $\rho_b = \rho^*, \rho_b = 0.5\rho^*, \rho_b = 0.1\rho^*,$ and $\rho_b = 0$. The aggregates are observed using a 40x Nikon Objective (NA = 0.6) for approximately 1 hour. During this time, we capture a series of 3000 frame videos at 20fps along the capillary.

Long-time dynamics: experiment set up

Next, we aim to measure the long-time dynamics and morphology of colloidal aggregates, over a period of 4 hour. For these experiments, the concentration of colloids is chosen such that, once the colloids have sedimented the surface area fraction is $18\% \pm 3\%$. We repeat the experiments at 6 *E. Coli* concentrations: $\rho_b = \rho^*, \rho_b = 0.5\rho^*, \rho_b = 0.2\rho^*, \rho_b = 0.1\rho^*, \rho_b = 0.05\rho^*$ and $\rho_b = 0$. The aggregates are observed using a 20x Nikon Objective for 4 hours; we capture one frame per minute time-lapses at 5 locations along the capillary.

Aggregate Tracking

To study the dynamics of colloidal aggregates, we develop tracking software in MATLAB. In each frame, we extract the center of mass, surface area, and perimeter of each aggregate from the binary image. Additionally, for aggregates where the major axis is significantly greater than the minor axis, we can reliably track their orientation by taking the angle between the major axis and the horizontal. Aggregates can be linked from one frame to the next by searching the vicinity of their previous center of mass for an aggregate of similar shape and size; when a match cannot be found, we assume a collision has occurred and treat it as a novel particle. In this way, we are able to create a 2D trajectory for each aggregate.

To extract information about the diffusion and rotational diffusion of aggregates, we apply the aggregate tracking software to the videos taken in the short-time dynamics experiments. Using the trajectories obtained from aggregate tracking, we calculate a Mean Squared Displacement (MSD) and Mean Squared Angular Displacement (MSAD) up to $\Delta t = 5s$. To improve the statistics of the MSD and MSAD, we only consider trajectories longer than 1500 frames. For each particle, a diffusion coefficient, or rotational diffusion coefficient, is extracted from a linear fit between time and MSD, or MSAD [Fig. 2A inset, Fig. 2B inset]. These coefficients are binned by size R_G; the averages and standard deviations of these bins are reported in Fig. 2A and Fig. 2B.

Similarly, we extract information of the Angular Velocity by tracking the aggregates observed in the long-time dynamics experiments. Angular Velocity is obtained through a linear fit between the aggregate orientation and time [Fig. 2D].

Inverted drop: experiment setup

We perform the colloidal aggregation experiment on the bottom surface of a hanging drop. In doing so, we are able reverse the fluid boundary condition at the interface where the experiment

takes place: a no-slip condition at the bottom of a glass capillary becomes a near perfect-slip liquid-gas condition at the bottom of a hanging drop. A 10 μL drop of the Colloidal Aggregation Solution, described previously, is suspended between a coverslip and a circular depression glass slide, as represented in Fig. S3A. We observe the apex of the drop, capturing a series of 3000 frame videos at 20 fps using a 20x Nikon objective. Following the tracking protocol described above, we extract information of the rotational dynamics of the aggregates from a linear fit between Orientation and Time for trajectories longer than 100 frames. We observe that 86% of clusters rotate counter clockwise [Fig. S3B], reversing direction from the previous experiments. These results are reminiscent of the findings of R. Di Leonardo et al [23], who find that *E. Coli* swim in counter-clockwise circles at a liquid-air interface, due to the perfect-slip boundary conditions, and confirm the role of the chirality of *E. Coli* flagella in the rotation of the colloidal aggregates. An exact mechanism for the torque transfer to the aggregates is outside the scope of this study.

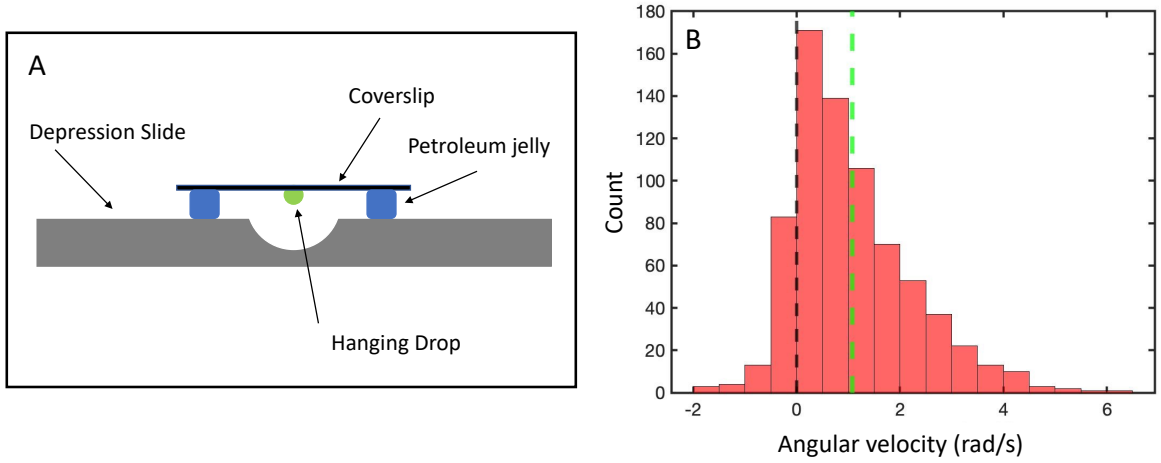

Figure S3 (A) Sketch of the experimental set up for the inverted drop experiment. (B) Distribution of Angular Velocities for all clusters tracked during the aggregation experiment on an inverted drop; the bacteria concentration is $\rho_B = 6 \times 10^8$ cells/mL.

Aggregate Morphology

Image Processing Techniques

First, we apply a gaussian filter to the image, with a standard deviation equal to the radius of a single colloid. Next, we binarize the image, and remove any regions touching the edge of the frame, to avoid analyzing the morphology of a partial aggregate.

Compare Aggregates with same Average Mass

One technique we use to compare the morphology of aggregates formed in baths with different activities is to find frames where the average mass of the aggregates is equivalent. Below, we compare aggregates formed in the thermal bath ($\rho_B = 0$) after 25 hours with aggregates formed in the highest activity bath ($\rho_B = \rho^*$) after 1.25 hours. In both cases, the average aggregate mass is 150 colloids. We observe aggregates in the thermal bath form ramified, branched structures. Aggregates in the active bath form compact structures.

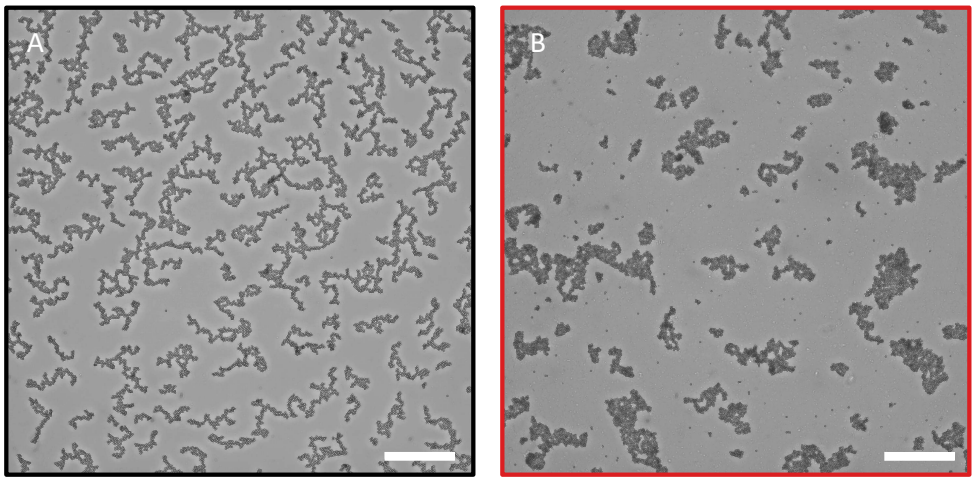

Figure S4 (A) Aggregates formed in the thermal bath ($\rho_B = 0$) after 25 hours. (B) Aggregates formed in the highest activity bath ($\rho_B = \rho^*$) after 1.25 hours. In both cases, the average aggregate mass is 150 colloids and the scale bar indicates 100 μm

Fraction of Colloids on the Boundary

We further quantify the morphology of the colloidal aggregates by analyzing the fraction of colloids on the boundary. Before we can analyze the fraction of colloids on the boundary of each aggregate, we must estimate the total number of colloids and the number of colloids on the boundary.

The number of colloids on the boundary is estimated from the perimeter of the binary region. The perimeter is calculated from the sum of the displacements of the pixels on the boundary of the binary region, including both interior and exterior boundaries. We estimate the number of colloids on the boundary as the total perimeter divided by the colloid diameter. Next, we estimate the total number of colloids to be the number of pixels in the binary region divided by the area of the Wigner-Seitz primitive cell for a hexagonal lattice. To verify these estimates, we perform a case study on a handful of small aggregates where it is possible to count the number of colloids manually. We find good agreement between the estimated value and the exact value for both the number of colloids on the boundary and the total number of colloids in an aggregate. The fraction of colloids on the boundary, presented in Fig. S6, is the ratio of the estimated number of colloids on the boundary and the estimated total number of colloids.

In Fig. S6, we compare the fraction of colloids on the boundary of aggregates assembled in four different active baths, corresponding to $\rho_b = \rho^*, \rho_b = 0.5\rho^*, \rho_b = 0.2\rho^*$, and, $\rho_b = 0$. To maintain consistency, we analyze frames where the average aggregate mass is equal to 150 colloids. We find that the fraction of colloids on the boundary decreases with increasing bacteria concentration.

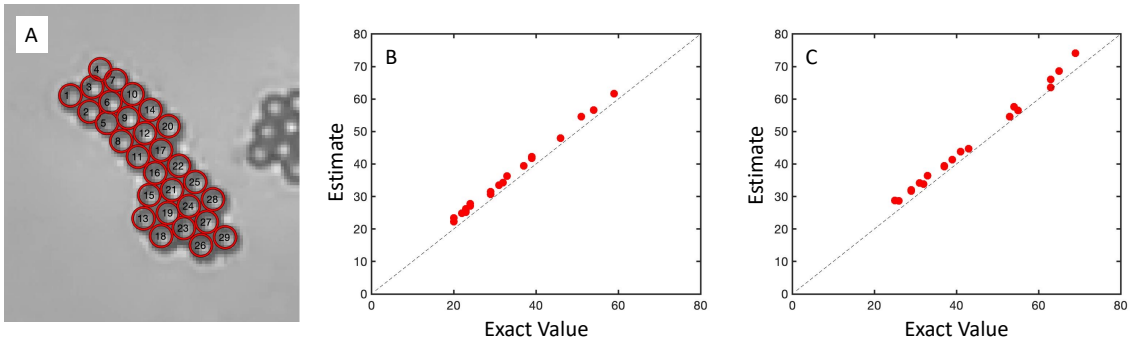

Figure S5 (A) Example of an aggregate where each colloid has been identified and labeled. The total number of colloids and number of colloids on the perimeter are counted manually. (B) The number of colloids on the perimeter, estimated from the perimeter of the binary region, compared with the exact value. (C) The total number of colloids in a cluster, estimated from the area of the binary region, compared with the exact value.

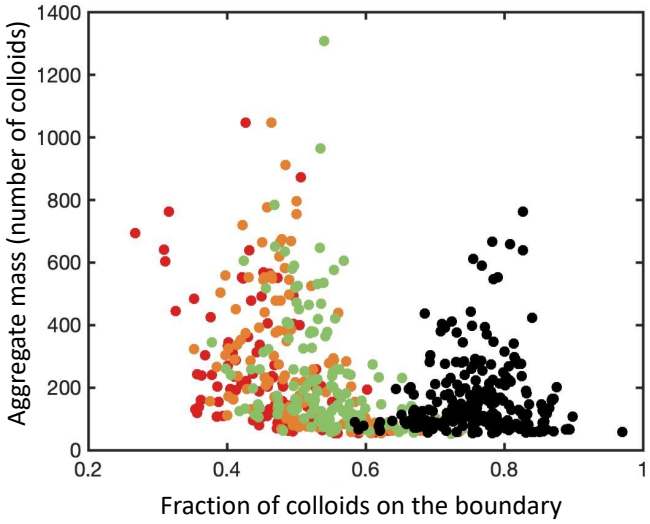

Figure S6 Fraction of colloids on the boundary for aggregates formed in various bacterial baths, estimated using the perimeter (interior and exterior) and area of the binary region. The bacteria concentrations are: $\rho_B = \rho^*$ (red) , $\rho_B = 0.5\rho^*$ (orange) , $\rho_B = 0.2\rho^*$ (green), and $\rho_B = 0$ (black).

Fractal Dimension

Taking inspiration from [25], we first quantify the morphology of the aggregates by calculating the Fractal Dimension. Using the list of pixels in each binary region, we calculate the Radius of Gyration of each aggregate using the following formula:

$$R_g^2 = \frac{1}{n}\sum_{i=1}^{n}(x_i - x_{cm})^2 + (y_i - y_{cm})^2$$

where (x_i, y_i) specifies the location of each pixel, and (x_{cm}, y_{cm}) specifies the center of mass of the binary region.

To calculate the average fractal dimension in a frame, we plot on Log-Log the Radius of Gyration and Binary Area for each aggregate in the frame; the slope gives the Fractal Dimension, as depicted in Fig. 3A. The equation relating Radius of Gyration and Aggregate Mass is displayed below, where m is the mass of a single colloid, a the radius, and ν the fractal dimension.

$$\frac{M}{m} = \left(\frac{R_g}{a}\right)^{\nu}$$

The Fractal Dimension as a function of time, obtained by analyzing the 4 hour aggregation experiments, is displayed in Fig. S7. We observe that the fractal dimension reaches a steady state value after about 2 hours.

Aggregate Mass Distribution

Experiment: We analyze the mass distributions of aggregates formed in the thermal bath, with $\rho_b = 0$ and the concentration of PEO = 3.25g/L. While we limit experiments in the active bath to 4 hours, beyond which the swimming velocity of the bacteria can reduce, experiments in the thermal bath can be extended up to 40 hours, to form larger aggregates. At various

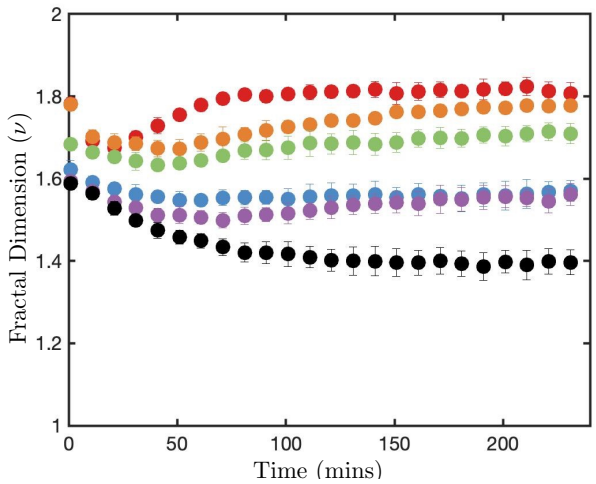

Figure S7 Fractal Dimension over time, for aggregates formed in various bacteria baths. The bacteria concentrations are: $\rho_B = \rho^*$ (red) , $\rho_B = 0.5\rho^*$ (orange) , $\rho_B = 0.2\rho^*$ (green), $\rho_B = 0.1\rho^*$ (blue), $\rho_B = 0.05\rho^*$ (purple), and $\rho_B = 0$ (black)

time-steps (2.5 hours, 5 hours, 10 hours, 25 hours, and 40 hours), we analyze 5 images from different locations along the capillary, using the binary image processing techniques described previously. Next, we calculate a empirical cumulative distribution function (or, eCDF), only considering aggregates greater than size 5 colloids.

$$eCDF(m) = \frac{\text{number of aggregates with mass} < m}{\text{total number of aggregates}}$$

the results of this analysis are summarized in Fig. S8A. We display the Survival Function, or 1-eCDF(m) that constitutes the probability of an aggregate to be of size larger than m. We find that the mass distribution follows a log-normal distribution, and can be made self-similar when normalized by the average aggregate mass [Fig. S8A], as expected for a thermal system [26]. We extend the result to additional experiments at lower depletant concentrations, corresponding a concentration of PEO of 1.6g/L, 0.8 g/L, and 0.6 g/L; again, we find the mass distribution is approximately log-normal [Fig. S8B]. We follow a similar protocol to obtain the survival function in the active bath at different bacteria concentration ρ_B , or internal torque, plotted on Figs. 3B and 3G respectively.

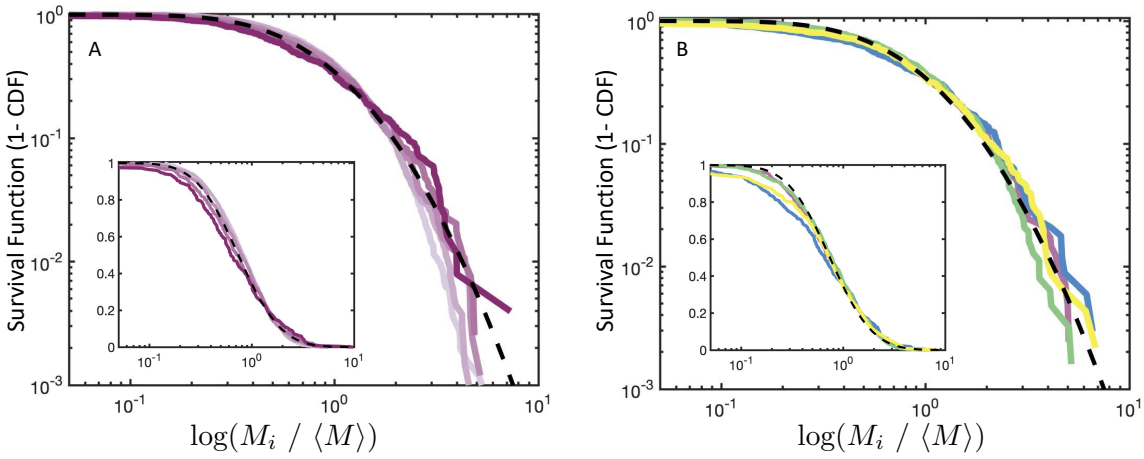

Figure S8(A) Survival Function (1-eCDF) of normalized aggregate mass, for the experimental conditions $\rho_B = 0$ and 3.25g/L PEO (MW 600k). Different times during the experiment are plotted on a gray to purple color palette : 2.5 hours (gray), 5 hours, 10 hours, 25 hours, and 40 hours (purple). (B) Survival Function (1-eCDF) of normalized aggregate mass after 24 hours, for varying concentrations of PEO depletant, with $\rho_B = 0$. Concentrations of PEO are: 3.25 g/L (purple), 1.6g/L (blue), 0.8g/L (green) and 0.6g/L (yellow). In both (A) and (B) the same data is plotted on a Log-Lin scale in the inset. The black dashed line corresponds to a log-normal distribution with $\mu = -0.3$ and $\sigma = 0.75$

Theory: In thermal (passive) systems of aggregation the growth dynamics of aggregates can be typically described by the Smoluchowski coagulation equation [36], which is a kinetic master equation for the formation and fragmentation probability of an aggregate or particle over time:

$$\partial_t \rho(\nu, t) = \tfrac{1}{2} \int_0^\nu \beta(\nu', \nu - \nu')\rho(\nu', t)\rho(\nu - \nu', t)d\nu' - \int_0^\infty \beta(\nu, \nu')\rho(\nu, t)\rho(\nu', t)d\nu'$$

where $\rho(\nu, t)$ denotes the size distribution function of aggregates of size (ie: mass) ν at time t. The key quantity that determines the kinetics of aggregate sizes is then given by the collision rate $\beta(\nu_i, \nu_j)$ for the merging of two aggregates with masses ν_i and ν_j, which depends generically on the collision cross-sectional area and aggregate diffusivity [26]:

$$\beta(\nu_i, \nu_j) \propto (R_i + R_j)(D_i + D_j)\,,$$

where R_i and D_i are the radius and diffusion coefficient of the i-th aggregate, respectively.

For passive aggregation processes, such as in Brownian coagulation, the aggregate mass distribution calculated from the Smoluchowski equation attains a self-preserving, scale-invariant form, which is well-described by a log-normal distribution [26] for the normalized aggregate mass $x \equiv m/\langle m \rangle$:

$$\rho(x) = \frac{1}{\sigma x \sqrt{2\pi}} \exp\left(-\frac{(\ln x - \mu)^2}{2\sigma^2}\right)$$

with mean μ and standard deviation σ. Interestingly, this scaling solution appears to be a universal feature in systems dominated by merging and fragmentation events, as it has been shown to describe the evolution of precursor cells and their progeny during tissue development [38], a biological process that is evidently far from equilibrium.

We also find that, both in experiments and simulations, the size distribution of colloidal aggregates in the absence of the bacterial bath is remarkably well-described by a log-normal distribution [Figs. 3B,3G]. Additionally, the distribution remains conserved over time and depletant concentration [Figs. S8A, S8B]. In contrast, we observe significant deviations from this universal scaling for the active bath, where increasing activity leads to the emergence of notable tails in the distribution. We note that even in thermal aggregation and fragmentation processes, the log-normal shape of the aggregate size distribution can only be obtained by numerically evaluating the Smoluchowski rate equation with suitable collision kernels and analytically by simplifying approximations [26]. However, for the active bacterial bath, a notable deviation from this log-normal form should be at least theoretically expected for the active bacterial bath because the collision rate $\beta(\nu_i, \nu_j)$ of two aggregates is now not only controlled by the diffusion coefficient and collision diameter of the aggregates, but by their active rotation as well, which effectively increases their cross-sectional area and thus leads to an increased probability for merging events. This effect, arising from the active rotation of aggregates, can be described by modifying the effective radius R or diffusion coefficient D of a aggregate, which we ad-

dress below to describe the mean aggregate mass evolution over time (see section: Aggregate Growth Model). The spinning kinetics induced by bacterial density thus provides a key microscopic departure from equilibrium behavior that is reflected in the global statistics of aggregate growth.

Aggregate Growth Model

Here we provide simple dimensional arguments to estimate the dynamics of the mean aggregate mass for both the thermal and active systems. First we start by considering the thermal case and note that the rate of change of the mean aggregate mass M should generically follow

$$\frac{dM}{dt} \propto M * D * C \tag{1}$$

where we assume the collision rate of two aggregates to be proportional to the density of aggregates C times their diffusivity D. We can now re-write the density of aggregates as

$$C = \frac{m\phi}{Ma^2}$$

where m and a are the mass and area of a single colloid, respectively, and $\phi \equiv n_c a^2/L^2$ is the surface fraction of colloids with the number of colloids n_c and the system size L. With the Stokes-Einstein relation for the diffusion coefficient of a single aggregate $D \propto k_B T/R_g$, where R_g denotes the radius of gyration, we obtain

$$\frac{dM}{dt} \propto \frac{m\phi}{a^2}\frac{k_B T}{R_g}$$

using the scaling relationship $M/m \propto (R_g/a)^\nu$, where ν denotes the fractal dimension of a typical aggregate, we are able to rewrite the equation in terms of the average mass, M:

$$M^{1/\nu} dM \propto \left(\frac{\phi k_B T m^{(\nu+1)/\nu}}{a^3} \right) dt$$

from which, by integration we obtain:

$$\frac{M}{m} \propto \left(\frac{\phi k_B T}{a^3} t \right)^{\alpha}$$

with the scaling exponent $\alpha = \frac{\nu}{\nu+1}$. For the thermal case with a fractal dimension of $\nu \simeq 1.4$, this indicates that the average aggregate mass grows as $M \propto t^{\alpha}$ with $\alpha \simeq 0.58$, in line with the theory and simulations provided by Cerda et al. [25].

We now introduce a simple modification of the rate equation Eq. (1) to consider the influence of the active bath. We note that aggregates in the active bath exhibit a persistent rotation with an angular velocity that depends on the bacteria concentration [Fig. 2D-F]. The simplest assumption one can make for the growth dynamics of a rotating aggregate is that it would encounter and accumulate additional colloids from the bath due to its active rotation, which then increases its collision rate. At a small time interval dt a rotating, rod-like aggregate with angular velocity Ω would perform an angular displacement of $\theta = \Omega dt$, and thus sweep an additional area of $\tilde{A} = \Omega R_g^2 \, dt$ as a consequence of its active motion. From a dimensional perspective, we can thus introduce an activity-dependent term $\lambda \equiv \Omega R_g^2 / D$ which would effectively increase the collision rate in Eq.(1). The simplest form of the aggregate mass rate equation could then be given by

$$\frac{dM}{dt} \propto CDM(1+\lambda) = \frac{m\phi}{a^2} \frac{k_B T}{R_g} \left(1 + \frac{\Omega R_g^3}{k_B T} \right) .$$

Inserting the experimentally obtained relation for the angular velocity $\Omega \propto \rho_B M^{\frac{\nu-3}{\nu}}$ [Fig. 2I], where ρ_B is the bacteria concentration and M the aggregate mass, we finally obtain

$$\frac{dM}{dt} \propto \mathcal{A} M^{-1/\nu} \left(1 + \mathcal{B} M \right) , \tag{2}$$

with the prefactors $\mathcal{A} = \phi k_B T m^{1+1/\nu}/a^3$ and $\mathcal{B} = \rho_B a^3/(k_B T m^{3/\nu})$. By integrating Eq. (2) we can obtain the growth dynamics of the average aggregate mass over time. For $\mathcal{A} = 1$ and different values of the activity-dependent parameter $\mathcal{B}$ we obtain the profiles shown in Fig S9, where for $\mathcal{B} = 0$ we recover the thermal scaling with the exponent $\alpha \simeq 0.58$. With increasing $\mathcal{B} > 0$ for the active cases, the exponent α increases monotonically; this displays the importance of the chiral active bath in increasing the rate of aggregation.

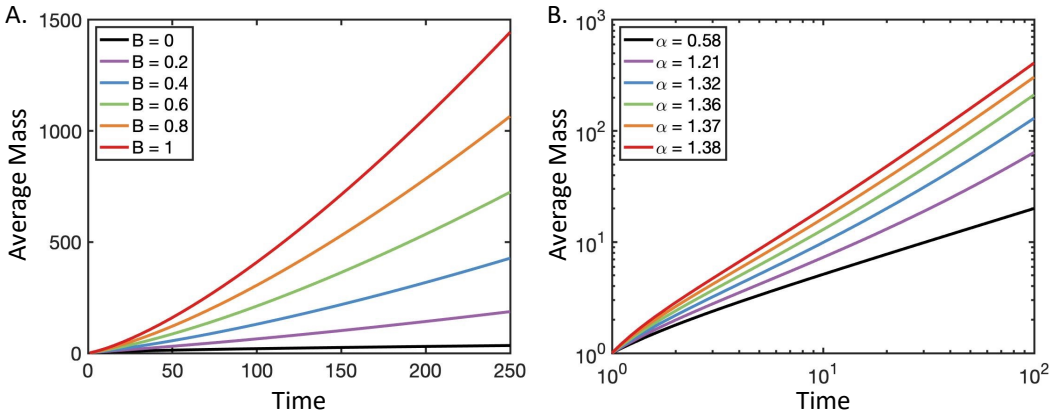

Figure S9 Evolution of the average aggregate mass as a function of time for different values of the activity parameter $\mathcal{B}$. (A) plotted on a linear - linear scale and (B) plotted on a logarithmic scale. Over a limited temporal range, the growth dynamics shows a scaling $M \propto t^{\alpha}$ with exponents given by $\alpha \simeq 0.58$ for $\mathcal{B} = 0$ (thermal), and increasing α for increasing values of $\mathcal{B} > 0$.

Aggregate Comparison

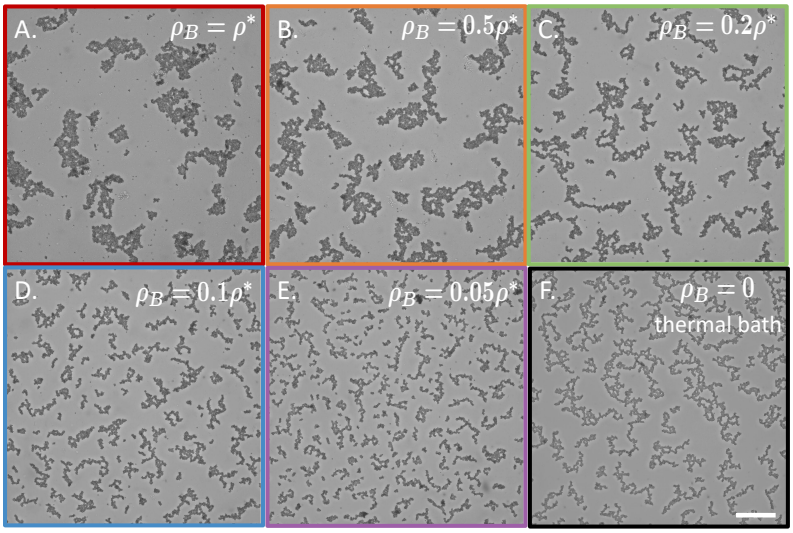

Figure S10 (A-E) Aggregates formed in the active bath after 4 hours, labeled with the corresponding bacteria concentration. (F) Aggregates formed in the thermal bath after 40 hours. The scale bar is 100um. Same scale for all.

Simulations

Computational model

In our computational model, colloids are modeled as two-dimensional particles, similarly to [39]. They interact through a sum of a repulsive interaction, enforcing volume exclusion, and an attractive interaction, representing the depletion force from experiments. The repulsive interaction is obtained through a Weeks-Chandler-Anderson potential (first line in the equation below), while attraction is obtained by a simple cosine-squared potential (second line):

$$U_{\mathrm{c}}(R) = \begin{cases} \epsilon_{\mathrm{c}} \left[\left(\frac{\sigma}{R}\right)^{12} - 2\left(\frac{\sigma}{R}\right)^{6} \right] & \text{if } R < \sigma \\ -\epsilon_{\mathrm{c}} \cos^2\left(\frac{\pi(R-\sigma)}{2r_{\mathrm{a}}}\right) & \text{if } \sigma < R < \sigma + r_{\mathrm{a}} \\ 0 & \text{if } R \geq \sigma + r_{\mathrm{a}} \end{cases} . \tag{3}$$

Here, ϵ_{c} is the attraction strength, σ is the particle diameter, R is the distance between the centers of the two particles, and r_{a} is the range of attraction. We choose $\epsilon_{\mathrm{c}} = 20\,k_{\mathrm{B}}T$ and $r_{\mathrm{a}} = 0.15\,\sigma$: these values correspond to a slightly softer potential than the one estimated for experiments, but, while still representing a strong short-range interaction and leaving the physics unchanged, they make simulations much more efficient and allow to simulate longer times.

To be able to define an angular velocity for the particles, and for the particles to be able to exchange angular momentum, we introduce some friction along the surface of the particles (see for instance [40]). We do so by coating each particle with 5 patches, positioned at distance $0.5\,\sigma$ from the particle center and equally spaced on the circumference (see Fig. S11). The number of patches, 5, was chosen so as to avoid any fictitious source of crystalline symmetry (namely, triangular symmetry with 3 patches, square with 4, or hexagonal with 6). Friction takes the form of a patch-patch interaction, that we chose to be mildly repulsive and of cosine-squared shape:

$$U_{\mathrm{p}}(r) = \begin{cases} \epsilon_{\mathrm{p}} \cos^2\left(\dfrac{\pi}{2}\dfrac{r}{r_{\mathrm{p}}}\right) & \text{if } r < r_{\mathrm{p}} \\ 0 & \text{if } r \geq r_{\mathrm{p}} \end{cases} . \tag{4}$$

Here, $\epsilon_{\mathrm{p}} = 10\,k_{\mathrm{B}}T$ is the patch-patch repulsion strength, r is the distance between two patches, and $r_{\mathrm{p}} = r_{\mathrm{a}} = 0.15\,\sigma$ is the patch-patch interaction range. Note that when two patches superimpose, the interaction energy between two colloids can stay negative as $\epsilon_{\mathrm{c}} \gg \epsilon_{\mathrm{p}}$. Patches move rigidly with the colloid they are attached to. This is ensured, at each time step, by summing the the forces acting on the central particle and on the 5 patches of the rigid body to obtain a force acting on their center of mass and a torque relative to their center of mass.

If the whole colloid has mass m, the central particle has mass $0.6\,m$ and each of the 5 patches has mass $0.08\,m$. This makes the moment of inertia of the colloid equal to that of a sphere, namely $\frac{2}{5}m(\frac{\sigma}{2})^2$.

Colloids are made spin by applying to each of them independently a torque of magnitude

τ, between 0 and $15\,k_{\mathrm{B}}T$. The torque results from a pair of forces of constant magnitude $f = \tau/(0.5\,\sigma)$; one applied to the center of the colloid and one to one of the patches, as shown in Fig. S11A. Fig. S11B shows all the forces applied to two colloids at contact (excluding thermal noise, discussed below).

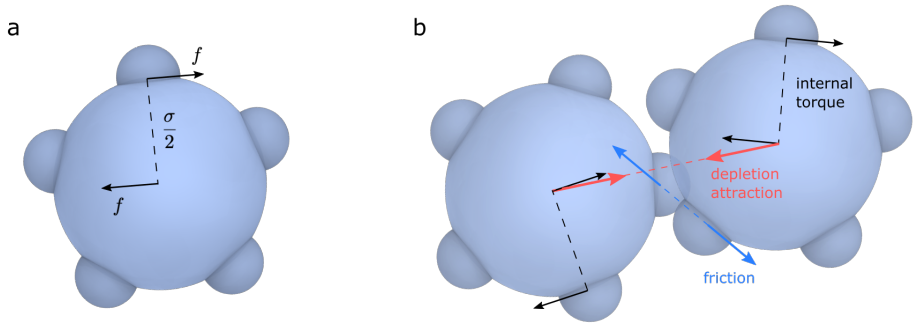

Figure S11 (a) Sketch of a colloid within our computational model. The 5 patches are rigidly attached to the central body. Their size represents the repulsion range $r_p = 0.15\,\sigma$. In black, the forces responsible for the active torque. (b) Two colloids interacting through central interactions (Eq. 3, in red) and patch-patch friction (Eq. 4, in blue). Those eventually result in an almost-rigid rotation of the two-body complex about their center of mass.

Simulation details

At the beginning of each simulation, particles are positioned at random sites of a square lattice, defined such that the surface density of colloids is the desired one. The initial orientation of particles is also randomized.

Two-dimensional molecular dynamics simulations are run in LAMMPS [41] and visualised with OVITO [42]. A velocity-Verlet integrator is coupled with a Langevin thermostat, mimicking an implicit solvent, so that the system is effectively in the NVT ensemble. The time step chosen for the integration of the 2D equations of motion is $\tau_s = 0.008\,\tau_0$, where $\tau_0 = \sqrt{m\sigma^2/(k_{\mathrm{B}}T)}$ is the simulation unit of time. The Langevin thermostat has a friction coefficient $\gamma = 0.08\,m/\tau_0$, meaning that the momentum of a particle relaxes on a scale of the order of

10 time steps. Such fast relaxation brings simulations close to the fully Brownian regime and favors computational stability.

Simulations of folding aggregates (Figs. 3D, 3E, 3F, 3G, 4B, 4C, 4E, 4F, 5A, 5B and Movies S3-S6) containing $N = 10000$ colloids were run in a square box with periodic boundary conditions, applied along both Cartesian directions. For surface density $\rho = 0.20\,\sigma^{-2}$, corresponding to a packing fraction $\phi = \rho \cdot \pi(\sigma/2)^2 \simeq 0.16$, 16 realizations, differing by the random number generator seed, were run for $5 \cdot 10^6$ time steps τ_s. Fig. 3D and 3E are screenshots taken at times $8 \cdot 10^3$ and $1 \cdot 10^5\,\tau_s$. Figs. 3F and 3G refer to time $3 \cdot 10^4\,\tau_s$, chosen so as to match approximately the sizes of the aggregates seen in the experimental time range. The folding dynamics is best described by Movies S5 and S6 and by Fig. S12.

Longer simulations were needed to fill the phase diagram of Fig. 5A, to ensure that at long times aggregates did not aggregate into percolating structures or, vice versa, that percolated structures did not break down into isolated aggregates: for each value of packing fraction shown (corresponding to density 0.10, 0.15, 0.20, 0.25 and 0.40 σ^{-2}), 2 different realizations were run for times between 2 and $9 \cdot 10^7\,\tau_s$ (the largest times being needed for low densities or when close to the transition).

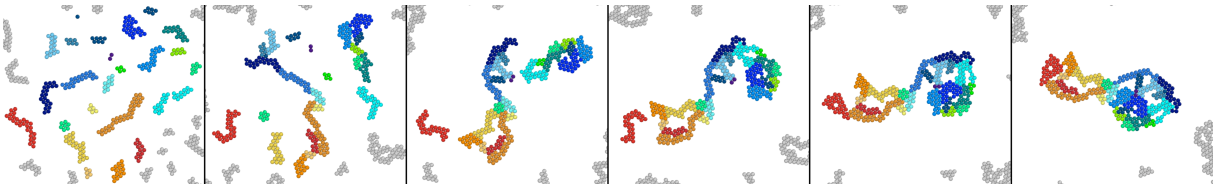

Figure S12 Aggregation and folding of an aggregate in simulations, with an internal torque of $10\,k_{\mathrm{B}}T$. Snapshots are taken at equally spaced times between 1 and $6 \cdot 10^4\,\tau_s$.

Simulations of non-folding aggregates (Figs. 4D, 4G, 4H) were performed running a clustering algorithm every 100 time steps and freezing aggregates, so that once a new particle binds it moves rigidly with the rest of the aggregate. The cutoff distance for the clustering algorithm

was $R = \sigma + r_a = 1.15\,\sigma$, corresponding to the interaction range. Within our setup, this procedure was incompatible with periodic boundary conditions in LAMMPS. As a consequence, simulations were run in a box delimited by an impenetrable wall, modeled by a purely-repulsive 6-12 Lennard-Jones interaction, with parameters $20\,k_BT$ and $1\,\sigma$, cut and shifted at its minimum. The number of colloids was however increased to $N = 100000$ to reduce the effect of hard boundaries, which was checked for with the aid of additional simulations with $N = 20000$ only, as shown in Fig. S13. In addition, data was discarded when the mass of the largest aggregate went beyond 10% of the total mass in the system.

Finally, inhibiting folding necessarily means forbidding particles from rolling on each other upon binding, akin to velcro-coated colloids. This makes the branches of the aggregate look thinner (1 colloid thick) than in the folding case (2 colloid thick), as shown by a comparison between Figs. 4G and 4E. To correct for the fact that comparable structures are now formed with only half of the mass, surface density was reduced to $\rho = 0.10\,\sigma^{-2}$.

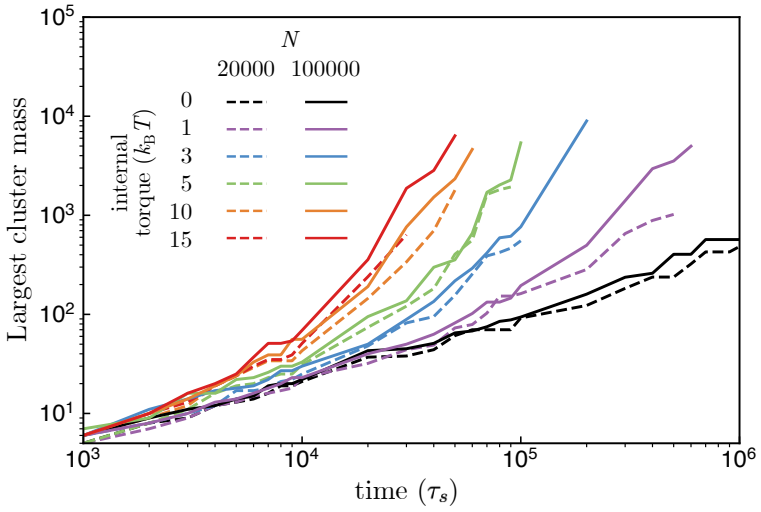

Figure S13 Time evolution of the larges aggregate size for non-folding simulations. Increasing the number of particles from $N = 20000$ (dashed lines) to $N = 100000$ (continuous lines) does not sensibly affect the measurement.

Stress-strain tests (Fig. 5C and Movies S7, S8) were run on gelled configuration taken from folding-aggregates simulations at density $\rho = 0.40\,\sigma^{-2}$ (i.e. $\phi = 0.31$), $N = 10000$ and time $1 \cdot 10^7\,\tau_s$. At such value of density, the system is in the gel phase for a wide range of activities, allowing us to compare gels prepared in very different conditions ($\tau = 0$, 1 and $3\,k_{\mathrm{B}}T$). The initial box size is $L_x = L_y = \sqrt{N/\rho} \simeq 158\,\sigma$. We stretch or compress it by $2\,\sigma$ at a time, in $10^5\,\tau_s$, then let the system equilibrate for $3 \cdot 10^5\,\tau_s$, and then average the measured stress tensor for $1 \cdot 10^5\,\tau_s$. We repeat this for 20 iterations, until a final strain of $40\,\sigma$ (i.e. 24%). For each value of internal torque used to prepare the initial gels, we use 3 different gel networks, deformed both along x and y, with 4 different seeds, so that each point shown in Fig. 5C is an average of 24 measures. The deformation runs are performed at no activity.

Data analysis

We run a **cluster analysis** and compute **gyration radii** through OVITO [42]. Two colloidal particles are considered in the same aggregate if their centers are within attraction range ($R < \sigma + r_{\mathrm{a}} = 1.15\,\sigma$).

The **fractal dimension** ν is computed by fitting masses M and gyration radii R_{g} to the scaling law $M \sim R_{\mathrm{g}}^{\nu}$, as shown in Fig. 3F. When computing R_{g}, we assume colloidal particles to be point-like, with (unit) mass concentrated at their center. For the inset of Fig.5A, we compute ν from the last 4 time frames of the simulations when the phase is cluster-like, and from the last 4 time frames before percolation when the phase is gel-like. We then fit the boundary between the two phases in the (ν, ϕ) space to the curve $\nu = 2 + \alpha \log(\phi)$ and find $\alpha \simeq 0.29$, as described in the main text.